In Situ IR Spectroscopy of Mesoporous Silica Films for Monitoring Adsorption Processes and Trace Analysis

*Bettina Baumgartner, Jakob Hayden, Andreas Schwaighofer, Bernhard Lendl**

Research Division of Environmental Analytics, Process Analytics and Sensors, Institute of Chemical Technologies and Analytics, Technische Universität Wien, Getreidemarkt 9, 1060 Vienna, Austria

KEYWORDS porous materials, infrared spectroscopy, functional coatings, sensor, thin film

ABSTRACT Adsorption of molecules on high-surface-area materials is a fundamental process critical to many fields of basic and applied chemical research; for instance, it is among the simplest and most efficient principles for separating and remediating polluted water. However, established experimental approaches for investigating this fundamental process preclude *in situ* monitoring and thus obtaining real-time information about the ongoing processes. In this work, mid-infrared attenuated total reflection (ATR) spectroscopy is introduced as a powerful technique for quantitative *in situ* monitoring of adsorption processes and thus enrichment of traces of organic pollutants from aqueous solution in ordered mesoporous silica films.-The synthesis, functionalization, and characterization of two silica films with 3D hexagonal and cubic pore structure on silicon ATR crystals are presented. Benzonitrile and valeronitrile as model compounds for aromatic and aliphatic water pollutants are enriched in hydrophobic films, while the matrix, water, is excluded from the volume probed by the evanescent field. Enrichment times of <5 s are observed during *in situ* measurements of benzonitrile adsorbing onto the film from aqueous solution. The sensing system is calibrated using the Freundlich adsorption equation as calibration function. Enrichment factors of benzonitrile and valeronitrile within the film were determined to be >200 and >100, respectively, yielding detection limits in the low ppm range. Furthermore, fast and complete desorption of the analyte, ensuring reliable regeneration of the sensor, was verified. Lastly, we derive and experimentally validate equations for ATR spectroscopy with thin film adsorption layers to quantify the absolute mass of adsorbed pollutant in the film. The excellent agreement between recorded absorptions at target wavenumbers of the target analytes and corresponding simulations corroborates the validity of the chosen approach.

INTRODUCTION

Since the discovery of mesoporous silicas in the 1990s,[1] much attention has been given to these high-surface-area (>1000 m^2 g^{-1}) and structurally well-defined materials.[2–4] Large, accessible pore volumes, versatile surface chemistry (and hence manifold possibilities of functionalization), and tunable regular pore sizes within the mesoporous regime (2–50 nm)[5] of organosilicas have been exploited in various fields such as catalysis,[6–8] membranes and separation,[9] electrochemistry,[10] sensors,[11] optics,[12] and environmental technologies.[13] Across the diversity of applications, the basic working principle relies on the fundamental process of adsorption, i.e., the enrichment of a guest species at the surface of the adsorbent. Thus, deepening the understanding of adsorbent–adsorbate interactions would allow further exploitation of the potential of these fascinating materials, benefiting many scientific disciplines.

This also holds for the practical application of these materials in the removal of organic or inorganic pollutants by means of adsorption. Early pioneering work dealt with the accumulation of heavy metals and was later extended to toxic anions, dyes, aromatic hydrocarbons, pesticides, and pharmaceuticals.[14] Typically, adsorption isotherms are recorded via batch experiments. In this approach, a certain amount of adsorbate is added to an aqueous solution of the pollutant. After some time (minutes up to hours) or after equilibrium has been reached, the adsorbate is filtered off and the concentration of the remaining pollutant is determined, e.g., by liquid or gas chromatography coupled to an ultraviolet–visible (UV/VIS) detector.[15–18] This experimental approach allows studying the adsorption capacity of materials at equilibrium, but it only provides indicative information about the adsorption kinetics and rates, which are crucial for enabling practical applications of adsorbents.

In the context of *in situ* monitoring of chemical and physical processes, mid-infrared (mid-IR) spectroscopy is a powerful alternative.[19] It provides direct and specific molecular information for use in qualitative as well as quantitative analysis at high time resolutions on the scale of seconds. For liquid samples, measurements in attenuated total reflection (ATR) mode stand out for their simple sample handling requirements and the possibility of inline measurements.[20] The principle of ATR measurement is based on absorbance in the evanescent field that extends into the sample as the IR beam is totally reflected (see Scheme 1).

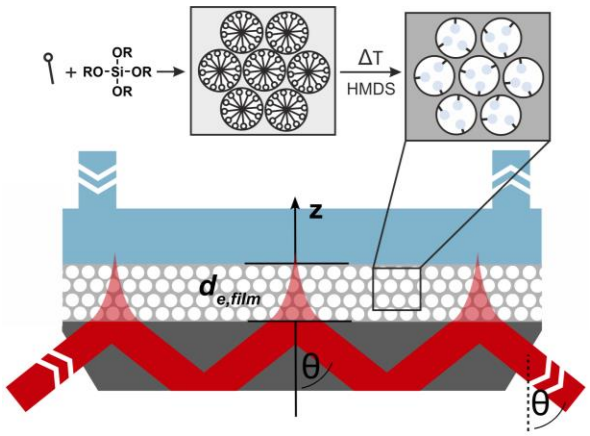

Scheme 1. Si ATR crystal (dark grey) coated with mesoporous silica film, obtained using the soft templating route and subsequent surface functionalization. IR absorbance takes place within the evanescent field (light red), which extends beyond the crystal into the film and, depending on the film thickness, into the sample solution flushed over the film.

To achieve the sensitivity required to target low concentrations of contaminants in water, a larger number of reflections at the crystal/sample interface can be used to increase absorption in the evanescent field and hence the sensitivity. This approach, however, is still limited by the strong background absorption of water. In the field of chemical sensing, a well-studied method for increasing the sensitivity of Fourier transform infrared (FTIR) spectroscopy towards organic contaminants in water while excluding water, which is a strong IR absorber is coating ATR crystals with hydrophobic materials.[21–24] Thereby, analytes are reversibly absorbed and concentrated in the region probed by the evanescent field, allowing limits of detection (LODs) in the mid-to-low ppb region to be reached for polymer films.[25] However, these polymer coatings rely on long enrichment and recovery times due to the diffusion resistance of bulk polymers, which limits their practical applications for *in situ* monitoring. Diffusion resistance and thereby response time can be reduced by the use of porous enrichment materials. In 1996, Lopez and co-workers used porous aerogels as enrichment films and could decrease the response time to a few seconds.[26] Similar efforts were reported for sensing of pesticides in water.[27] These analytical sensing applications focused on quantitative analysis of the solute in aqueous solutions but did not attempt to quantify the amount of solute dissolved or adsorbed in the different enrichment layers, which were composed of either polymers or metal oxides. Presumably, such quantification, particularly in the case of polymers, was hindered by difficulties in reproducible preparation and the poor stability of these layers.

In the latter respect, silica films outperform polymers in terms of mechanical stability, as these materials are not prone to swelling and can be covalently attached to the ATR crystal surface.[26] Today, using silica for enrichment films seems even more promising, as sol-gel chemistry has evolved significantly since then, allowing for precise pore design by means of templating methods[28] and production of highly reproducible film thicknesses.

In this contribution, we demonstrate for the first time the application of ordered mesoporous silica films in mid-IR ATR sensing of organic pollutants in water. We present the synthesis of

organically modified mesoporous silica films with two different pore structures and their comprehensive characterization via FTIR spectroscopy, X-ray diffraction (XRD), transmission electron microscopy, and contact angle measurements. Silica films were spin-coated on rectangular ATR crystals (20 × 10 × 0.5 mm) cut from low-cost, disposable silicon wafers to study the influence of the pore structure on the enrichment times and performance for the determination of nitriles in water. Valeronitrile and benzonitrile serve as model compounds for aliphatic hydrocarbons as well as toxic aromatic herbicides like bromoxynil, chloroxynil, dichlobenil, and ioxynil, which are applied on the scale of thousands of tons in agricultural and household use.[29] In the present system, the adsorption mechanism is described by Langmuir and Freundlich models. Finally, theoretical considerations allow the quantification of adsorbed molecules in milligrams per cubic centimeter (mg cm^{-3}) from recorded IR absorbance spectra, and these theories are confirmed via control experiments.

RESULTS AND DISSCUSSION

Synthesis and Characterization of Mesoporous Silica

Surface-modified mesoporous silica films were obtained using the surfactant templating route, using acidic hydrolysis and condensation of tetraethoxysilane (TEOS) in ethanol and cetyltrimethylammonium bromide (CTAB) as surfactant.[30] The 425 nm and 500 nm thick 3D hexagonal and cubic silica films, respectively, were obtained by spin-coating and subsequent simultaneous surfactant removal and surface functionalization with hexamethyldisilazane (HMDS) in abs. acetone. The presence of Si–O–Si stretching modes at ~1070 cm^{-1} in the ATR-IR spectra (Fig. 1) of the silylated films confirmed the formation of silica. IR absorption bands at 1259 cm^{-1} and 2900 cm^{-1} are associated with the CH_3 deformation and C–H stretching modes, respectively, and stem from the organic moieties introduced by the surface functionalization.

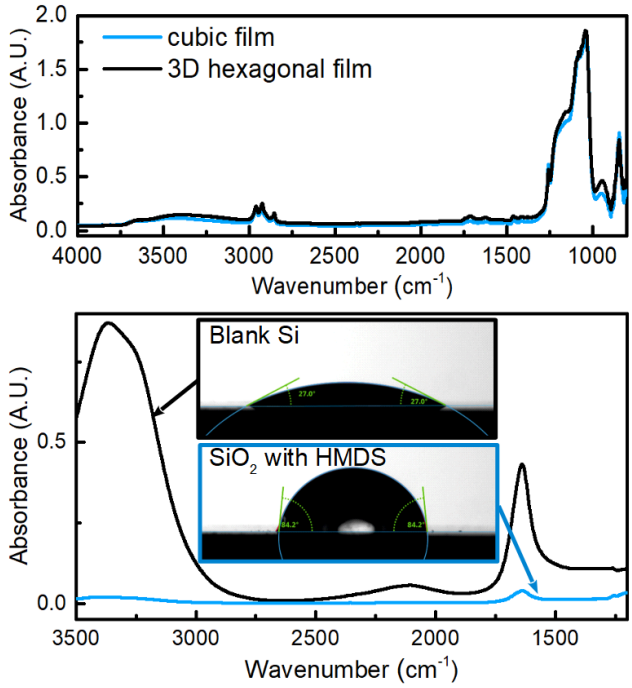

Figure 1. (Top) FTIR spectra of mesoporous hybrid films deposited on a Si ATR crystal: 3D hexagonal (black) and cubic (blue) film. Spectra were recorded with blank Si ATR crystals as background. (Bottom) FTIR spectra of water on blank (black) and coated (blue) Si ATR crystals: Organically modified mesoporous films repel water from the evanescent field, yielding strongly reduced IR absorption from water. Insets show photographs of contact angle measurements of (top) uncoated Si and (bottom) surface-modified mesoporous silica films. Surface modification increased the contact angles to 85°.

The surface wettability was characterized by static contact angle measurements. Surface modification led to an increase of the contact angle from 27° for unsylilated silica to 88° for organically modified silica films. The increased hydrophobicity of the sylilated silica film was further confirmed with ATR-IR spectra of water on coated and uncoated ATR crystals: Water is largely eliminated from the probed volume on coated ATR crystals compared to blank Si ATR crystals (see Supporting Information for spectra of unmodified silica). The IR absorption bands of water spectra in Fig. 1 at 3400 cm^{-1} and 1640 cm^{-1} are less intense for spectra recorded with coated ATR crystals compared to blank Si crystals. Note that the change in relative intensity of the water bands is a result of the wavelength dependency of the depth of penetration d_p of the evanescent wave (see Translation of IR Absorbance to Absolute Concentrations subsection).

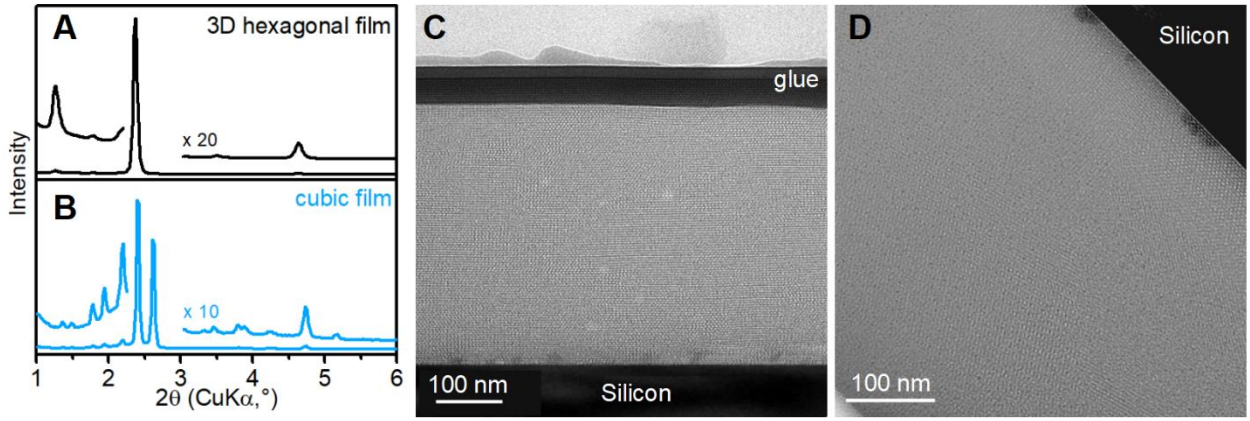

Figure 2. X-ray diffraction patterns of (A) 3D hexagonal and (B) cubic mesoporous films obtained in Bragg-Brentano geometry. Cross-section transmission electron micrographs of functionalized (C) 3D hexagonal-and (D) cubic-mesoporous films.

The variation of the CTAB/Si molar ratio as well as the optimization of the relative humidity (RH) during spin-coating led to 3D hexagonal and cubic films. XRD patterns at low angles for both structures are depicted in Fig. 2 and are in good agreement with the literature.[31–33] Transmission electron micrographs (Figs. 2C–2D) clearly show highly ordered pore structures throughout the film.

Characterization of Silicon ATR Crystal and Analytes

The Si ATR crystal provides maximum transmission in the range of 2000–2300 cm^{-1} (highlighted in blue in Fig. 3), while the transmission decreases below 1500 cm^{-1}, as illustrated in the single-channel spectrum in Fig. 3. This corresponds to a root mean squared

(RMS) noise of 100% lines of 4×10^{-5} AU for the region around 2100 cm^{-1} and a fourfold increase of the noise for the 1800–1400 cm^{-1} region (calculated from 32 averaged scans; see Supporting Information and Experimental Details section for more information). Within the range of–maximum transmission of the Si ATR crystal, the ν–C–N vibrational modes of benzonitrile (2238 cm^{-1}), valeronitrile (2257 cm^{-1}), and its toxic derivatives used as herbicides are found between 2260 cm^{-1} and 2220 cm^{-1}.

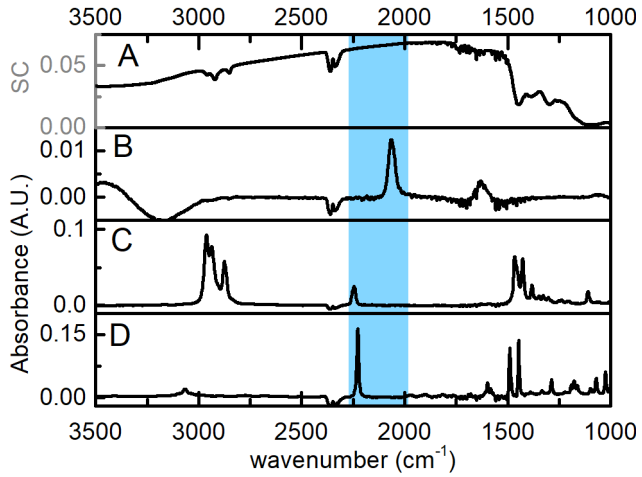

Figure 3. (A) Single-channel spectrum of uncoated Si ATR crystal and ATR-FTIR spectra of (B) aqueous NaSCN solution (10 g L^{-1}, water background, SCN band at 2010 cm^{-1}), (C) pure valeronitrile (ν–CN mode at 2257 cm^{-1}), and (D) pure benzonitrile (ν–CN mode at 2238 cm^{-1}). The maximum transmission of the ATR crystal is highlighted in blue.

In addition to organic pollutants, aqueous sodium thiocyanate solution (–SCN vibration mode at 2010 cm^{-1}) was applied on uncoated ATR crystals to act as a tracer substance. This tracer aids in determining the time needed to completely exchange the flow cell volume (see Adsorption/Desorption Studies of Benzonitrile Solutions subsection). This detour was necessary because even the concentrations of saturated benzonitrile and valeronitrile solutions are too low to be detected on uncoated ATR crystals due to the low solubility/absorption coefficients of these compounds.

Adsorption/Desorption Studies of Benzonitrile Solutions

The analyte solutions were applied via an automated flow system consisting of a peristaltic pump and a 10-way selection valve (see Scheme 2 in the Experimental Details section) that allowed for automated sample selection and reproducible sample injection. To study the speed of adsorption and desorption of benzonitrile on/from the silica film, a defined sequence of water, analyte in water, and water was applied in an automated way while recording one spectrum per second. Either 100 mg L^{-1}benzonitrile solution or 10 g L^{-1} NaSCN solution were used as analytes. Figure 4 shows the temporal progression of the integrated areas of the C–N and SCN bands, respectively.

An important step in this experimental setup is distinguishing the actual adsorption/desorption process from delays caused by the finite response time of the flow

system (flow cell, tubing). To achieve this, a reference solution of NaSCN was applied to an uncoated ATR crystal to give information about the dead time of the system as well as the time needed to completely exchange pure water with the analyte solution. The sample introduction step of the flow sequence is highlighted in gray in Fig. 4. The profile depicted in Fig. 4 shows that 90% displacement of water by analyte solution requires $t_{90\%}$ = 17 s, and flushing pure water for analyte removal until reaching 10% of IR absorbance requires $t_{10\%}$ = 17 s.

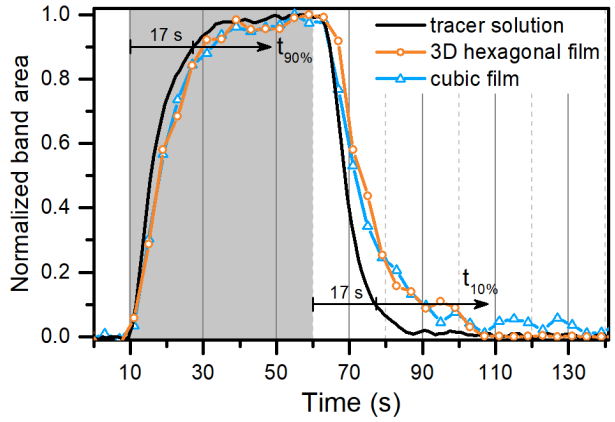

Figure 4. Adsorption/desorption profiles of 100 mg L^{-1} benzonitrile onto mesoporous silica films with 3D hexagonal and cubic pores. For comparison, the temporal concentration profile of the NaSCN tracer solution was recorded on uncoated Si ATR crystals and serves as indicator of the actual analyte dispersion in the flow cell. The gray box indicates the time period during which sample was pumped through the sample cell.

The profile of ~~the~~ adsorption of benzonitrile onto 3D hexagonal and cubic mesoporous films closely matches the profile of the NaSCN solution, and only a slight delay of 3 s ($t_{90\%}$ = 20 s) and 5 s ($t_{90\%}$ = 22 s) for $t_{90\%}$, respectively, can be observed. Desorption is significantly slower than adsorption, as indicated by the increase of $t_{10\%}$ for both films by 13 s ($t_{10\%}$ = 30 s) relative to the NaSCN reference measurement, which experienced no retention. For flow rates below 1 mL min^{-1}, slow exchange of the sample volume dominates. However, the flow rate had no effect on the absorption measured after equilibration in the range from 0.5 mL min^{-1} to 2 mL min^{-1} (see Supporting Information).

Both profiles illustrate the fast adsorption of benzonitrile into mesoporous silica films that has already been concluded from batch experiments,[16] but, to our knowledge, have never been recorded *in situ*. Furthermore, both structured films are fully recovered after desorption and the IR absorbance returns to its initial value.

Equilibrium Adsorption Experiments

Series of benzonitrile and valeronitrile solutions with concentrations ranging between 1 and 500 mg L^{-1} were applied in triplicate to determine the adsorption capacity of the silica films at equilibrium as well as the calibration function. To this end, a peristaltic pump was placed downstream of the flow cell to draw the sample solutions through the flow cell at 2 mL min^{-1}

for 2 min. Because the recorded absorbance scales linearly with the concentration of adsorbed nitriles (Lambert-Beer's law, Eq. 3), adsorption isotherms can be obtained directly from the band areas and are depicted in Fig. 5. The cubic film adsorbed more benzonitrile than the film with 3D hexagonally arranged pores. The same behavior is observed for valeronitrile, although the band areas are smaller due to the smaller absorption coefficient of the ν–CN vibration of this molecule.

For deriving a calibration function and comparing adsorption performance with the literature, the obtained adsorption data was described using the frequently employed Langmuir and Freundlich models. Whereas the Langmuir model (Eq. 1) assumes monolayer coverage, the Freundlich model (Eq. 2) describes multilayer adsorption with decreasing adsorption enthalpy. The models are expressed as

$$q_e = \frac{q_m K_L c}{1+K_L c} \quad (1)$$

$$q_e = K_F c^{\frac{1}{n}} \quad (2)$$

where q_e (AU cm^{-1} for data obtained from IR absorption bands; mg cm^{-3} for absolute concentrations obtained in the following section) is the amount of adsorbed analyte, q_m (AU cm^{-1} or mg cm^{-3}) is the maximum adsorption capacity, c is the concentration of applied analyte solutions (mg L^{-1}), K_L (cm^3 mg^{-1}) is the Langmuir constant, K_F (AU cm^{-1} [mg L^{-1}]$^{-1/n}$; or mg cm^{-3} [mg L^{-1}]$^{-1/n}$) is the Freundlich affinity coefficient, and n (unitless) is the Freundlich linearity index. In our experiments, which were performed with sample continuously flushed over the film, c is equal to the applied concentration, which is different from c in batch experiments, where adsorption reduces the concentration in the solution.

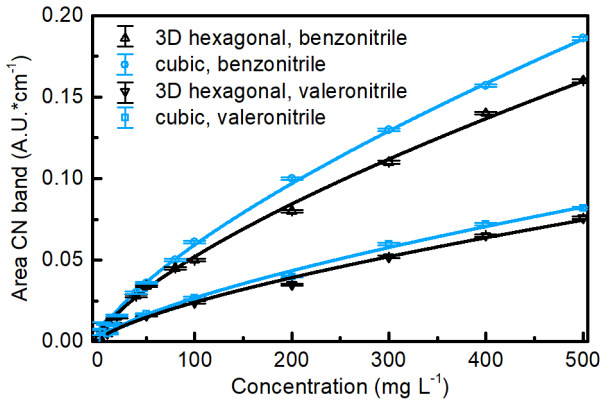

Figure 5. Adsorption isotherms of benzonitrile and valeronitrile solutions on 3D hexagonal and cubic mesoporous silica films obtained from CN band areas at different concentrations fitted with the Freundlich equation. The standard deviation was calculated from three consecutive measurements (see Supporting Information for data).

The experimental adsorption data was fitted with Langmuir and Freundlich isotherms and the obtained parameters are given in Table 1. The values of chi square (χ^2) are lower for the Freundlich model, indicating a better fit for this isotherm for both structures.[34]

Table 1. Isotherm parameters obtained by fitting the experimental data obtained for benzonitrile and valeronitrile to the Langmuir and Freundlich models.

	Analyte	Langmuir fit χ^2	Freundlich fit χ^2	K_F [AU cm^{-1} (mg L^{-1})$^{-1/n}$]	n
3D hexagonal film	benzonitrile	3.5×10^{-5}	6.3×10^{-6}	0.0021	1.44
	valeronitrile	1.3×10^{-5}	3.6×10^{-6}	0.0011	1.42
Cubic film	benzonitrile	1.8×10^{-5}	2.4×10^{-6}	0.0023	1.41
	valeronitrile	9.6×10^{-6}	2.6×10^{-6}	0.0009	1.39

Translation of IR Absorbance to Absolute Concentrations

So far, the data gained from the adsorption experiments via ATR spectroscopy presented in this study have been given in absorption units (AU) or band area (AU cm^{-1}). For comparison of the obtained parameters with other adsorption studies, translation to units commonly used in this field is beneficial. The determination of absolute adsorbed pollutant concentrations in, e.g., milligrams of pollutant per mass or volume adsorbate in the mesoporous films demands theoretical considerations.

(i) Determination of the Effective Path Length of the Blank Si ATR Crystal: The concentration of the analyte is directly proportional to the absorbance A according to Lambert-Beer's law:

$$A = \varepsilon\, c\, d \qquad (3)$$

where ε is the decadic molar absorption coefficient, c is the analyte concentration, and d is the path length. The path length applies to transmission measurements and corresponds to the effective path length d_e in ATR spectroscopy, which is defined as "the thickness of a film of the sample material that would give the same absorbance for transmission at normal incidence as that obtained in the ATR experiment."[20,35] For weakly absorbing samples, d_e can be approximated by

$$d_{e,\perp} = \frac{\lambda_0}{n_1} \cdot \frac{n_{21}\cos(\theta)}{\pi\,(1-n_{21}^2)[sin^2(\theta)-n_{21}^2]^{1/2}} \qquad (4)$$

$$d_{e,\parallel} = \frac{\lambda_0}{n_1} \cdot \frac{n_{21}\cos(\theta)[2\,sin^2(\theta)-n_{21}^2]}{\pi\,(1-n_{21}^2)[(1+n_{21}^2)sin^2(\theta)-n_{21}^2][sin^2(\theta)-n_{21}^2\,]^{1/2}} \qquad (5)$$

$$d_e = \frac{d_{e,\perp} + d_{e,\parallel}}{2} \tag{6}$$

where n_1 and n_2 are the refractive indices of the ATR crystal and the sample, respectively ($n_{ij} = n_i/n_j$), λ_0 is the wavelength of light, and θ is the angle of incidence of the IR beam relative to the surface normal. For an unpolarized IR beam, as generated by the globar source of the spectrometer used here, it is the average of the parallel and perpendicular effective path length (Eq. 6). For multi-reflection ATR crystals, as used in this study, the absorbance increases linearly with the number of active bounces N:

$$A = \varepsilon\, c\, d_e\, N \tag{7}$$

For a blank Si ATR crystal with N = 14, θ = 55°, n_1 = 3.42, n_2 = 1.33 (water), and λ_0 = 6.1 µm, Eq. 7 yields $N \times d_e$ (1640 cm^{-1}) = 4.23 µm. An experimentally determined value for d_e was obtained by comparing the intensity of the water absorption band at 1640 cm^{-1} measured using a transmission cell with defined path length and the ATR crystal. This led to an experimentally determined d_e of 4.2 µm (0.3 µm for one bounce), which is in good agreement with the theoretically obtained d_e.

(ii) Theoretical Evaluation of the Effective Path Length Within the Mesoporous Film: For coated ATR crystals, the definition of the effective path length necessary for retrieving adsorbed concentrations must take into account that the evanescent field extends beyond the film's thickness (see Scheme 1). Assuming that the IR absorption of the analyte in the bulk liquid covering the film is negligible, $d_{e,film}$ is found by scaling Eq. 8 by the fraction s of the evanescent field's intensity that is confined within the film and hence can be absorbed by adsorbed molecules:

$$d_{e,film} = d_e\, N\, s \tag{8}$$

$$s = \frac{\int_0^{th} I(z)dz}{\int_0^{\infty} I(z)dz} = 1 - e^{\frac{-2\,th}{d_p}} \tag{9}$$

$$I(z) = I_0\, e^{\frac{-2\,z}{d_p}} \tag{10}$$

$$d_p = \frac{\lambda_0}{2\pi\sqrt{n_1^2 \sin^2(\theta) - n_2^2}} \tag{11}$$

where I_0 is the incident power, th is the film thickness, z is the distance from the crystal surface, and d_p is the depth of penetration, which is defined as the distance from the ATR crystal at which the electric field falls to $1/e$ of the electric field at the interface. Note that even though d_p and d_e are both smaller than the film thickness, a fraction of the evanescent field reaches beyond the film and causes IR absorption within the bulk liquid.

When considering a refractive index n_2 = 1.26–1.37 for silica[36] (instead of water for the calculations on blank ATR crystals), the fractions of the evanescent wave within the film and their corresponding corrected effective path lengths $d_{e,film}$ are given in Table 2.

Table 2. Calculated parameters and effective path lengths within the mesoporous films.

	Wavelength λ_0 [µm]	d_p[a] [µm]	d_e[b] [µm]	s[c]	$d_{e,film}$[d] [µm]
3D hexagonal film	6.10	0.388	0.278	0.89	3.45
th = 425 nm	4.45	0.293	0.233	0.95	3.09
cubic film	6.10	0.388	0.278	0.92	3.59
th = 500 nm	4.45	0.293	0.233	0.97	3.16

[a] Depth of penetration, [b] effective path length, [c] fraction of the effective path length within the film, [d] effective path length within the film.

(iii) Experimental Verification of the Effective Path Length: The theoretically obtained effective path lengths were compared with absorbance measurements of nitrile rubber pressed on blank and coated ATR crystals. The nitrile rubber is sensed exclusively in the small fraction of the evanescent field that extends beyond the film. For the ν–C–N mode at 2230 cm^{-1}, this fraction (1 − *s*), as obtained using Eq. 9, is 5% and 3%, respectively, for the 3D hexagonal and cubic films. Consequently, the absorbance of the C–N band on the coated ATR crystals is expected to be reduced to 1 − *s* relative to the absorbance on uncoated crystals. The experimentally obtained absorbance fractions of 5.4 ± 0.8% and 4.3 ± 0.5% for hexagonal and cubic films, respectively, agree well with our theoretical projections. Therefore, one can reasonably assume that the theoretically obtained effective path lengths $d_{e,film}$ and hence the retrieved concentrations of adsorbed benzonitrile are in good agreement with the actual values.

(iv) Retrieval of Absolute Concentrations: The decadic molar absorption coefficients ε of benzonitrile and valeronitrile were determined by IR transmission measurements to be ε = 2350 AU L cm^{-2} mol^{-1} and ε = 1388 AU L cm^{-2} mol^{-1} for the ν–C–N mode of benzonitrile and valeronitrile, respectively. Absolute concentrations of the analyte within the film were obtained by inserting ε and $d_{e,film}$ into Lambert-Beer's law (Eq. 3); the results are depicted in Fig. 6.

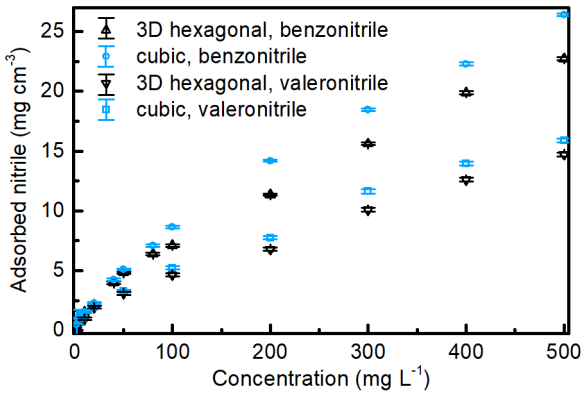

Figure 6. Adsorption isotherms of benzonitrile and valeronitrile solutions on 3D hexagonal and cubic mesoporous silica films obtained from Lambert-Beer's law.

As for solutions measured on uncoated ATR crystals, the derived theory yields analyte concentrations with respect to the matrix volume. For analytes present within the adsorption layer, this film constitutes the matrix, and hence concentrations are given relative to the adsorbent's volume. The absolute mass of adsorbed analyte can be retrieved by multiplication of the obtained concentration with the film's volume, which based on the known film thickness and probed area is 8.5×10^{-5} cm^3 and 1×10^{-4} cm^3 for the 3D hexagonal and cubic film, respectively. From that, the absolute mass of benzonitrile adsorbed from a 100 mg L^{-1} solution into the film was determined to be 7.4 mg cm^{-3} (0.63 µg per film) and 9.0 mg cm^{-3} (0.88 µg per film) for the 3D hexagonal film and the cubic film, respectively.

Figures of Merit of the Sensing System

With the parameters discussed in the previous sections, the LOD, response time, and enrichment factor can be evaluated as figures of merit for the presented continuous water monitoring sensor. Firstly, the fitting parameters of the Freundlich equation from Table 2 serve as calibration function. LOD can be determined using this function. Typically, LOD is defined as

$$LOD = \frac{3\sigma}{\frac{dq_e}{dc}(0)} \qquad (12)$$

where σ is the noise floor of the measured signal and $dq_e/dc(0)$ is the change in the signal with concentration at $c = 0$, i.e., the sensitivity. Because the sensitivity at $q_e(c = 0)$ is not defined for the Freundlich function, we define the LOD by $q_e(\text{LOD}) = 3\ \sigma$. The standard deviation σ of the band area is derived from consecutive 100% lines taken every 4 s (32 averaged scans, see Experimental Details section). Inserting the definition of LOD into Eq. 2 and solving for LOD, with the Freundlich parameters given in Table 1 and $\sigma = 10^{-3}$ AU cm^{-1}, yields LODs of 1.5 mg L^{-1} and 1.3 mg L^{-1} for benzonitrile and 8.4 mg L^{-1} and 6.6 mg L^{-1} for valeronitrile for the 3D hexagonal and cubic film, respectively.

To emphasize the accessibility of the important fingerprint region below 1800 cm^{-1}, we analyzed the bands of valeronitrile between 1500 and 1400 cm^{-1} that correspond to the δ–C–H vibrational modes of this molecule. LODs were calculated in the same manner and determined to be 9.6 mg L^{-1} and 5.0 mg L^{-1} for the 3D hexagonal and cubic film, respectively. Although the noise level within the fingerprint region is higher ($\sigma = 4 \times 10^{-3}$ AU cm^{-1}), the obtained LODs are nearly identical to the values given above due to the stronger absorption of these bands. Particularly noteworthy is that for many polymer-based coatings (the materials most widely used for ATR enrichment coatings) this region is not accessible due to the strong absorption of the coating itself.

Furthermore, a response time of <5 s can be deduced from the adsorption/desorption profiles shown in Fig. 4. The enrichment factor is defined as the ratio of the volumetric concentration in the film and the solution and for a 5 mg L^{-1} benzonitrile solution equals 200 and 210,

respectively, for 3D hexagonal and cubic films, while for a 10 mg L^{-1} valeronitrile solution it equals 100 for both films. Because the calibration function is not linear, the enrichment factor increases for lower analyte concentrations. Finally, we point out that the mesoporous silica-coated ATR crystals proved their robustness during extensive testing. Both films have been in use for several months and were exposed to several liters of aqueous solutions and show no decrease in performance in terms of adsorption/desorption behavior as monitored by FTIR spectroscopy or exfoliation. In clear contrast to frequently employed polymer coatings, mesoporous silica coatings resist organic solvents and do not swell, which allows performance of various cleaning procedures in case of fouling or use of analytes that cannot be removed with water.

CONCLUSION

In this study, we present a new approach for *in situ* monitoring and quantitative analysis of solutes adsorbed on high-surface-area materials. This is demonstrated via the use of two different ordered mesoporous silica thin films as enrichment layers in an ATR spectroscopic sensing system. The presented system comprises easily exchangeable ATR crystals from low-cost silicon wafers, which in contrast to commercial ATR crystals allow for fast and flexible screening of enrichment layers without the need to recover the blank ATR crystal between experiments. Application of other ATR materials such as germanium is possible and would broaden the accessible spectral range, thus allowing investigation of further applications where spectral information in the entire mid-IR range is required. The adsorption/desorption profiles of benzonitrile and valeronitrile, which were selected as surrogates/model substances for pesticides and aliphatic pollutants in water, were recorded *in situ* using an automated flow system. Thereby, response times of <5 s were observed for both pore structures and analytes, and complete recovery of the sensor was observed within 30 s. After calibration of IR absorption band areas using the Freundlich isotherm, limits of detection for nitriles in water were determined to be between 1 and 10 mg L^{-1} for both films with 4 s integration time. Isotherm data given in absorption units was translated into absolute mass of adsorbed pollutant in the mesoporous film using theoretical considerations. The calculated spectral signatures of material outside the coated ATR crystal were in good agreement with experimentally observed values. This finding has enabled us to quantify the absolute amount of adsorbed analyte by application of Lambert-Beer's law. Consequently, results obtained via the proposed ATR-IR spectroscopic method could be directly compared with adsorption experiments commonly performed in the batch approach. The adsorbed concentrations within the film obtained in this manner correspond to volumetric enrichment factors of up to 210 for accumulation of nitrile from water.

In conclusion, the results presented in this study demonstrate that ordered mesoporous silica is a highly suitable material for enrichment films in ATR-IR spectroscopy. Considering the great versatility of mesoporous silica in terms of pore design and functionalization, this material holds great promise for sensing diverse organic contaminants in water and may be applicable to many more analytical challenges. For material designers, *in situ* monitoring of adsorption and desorption into and out of the material at a temporal resolution of seconds delivers valuable information for development and understanding of novel porous materials.

EXPERIMENTAL DETAILS

Materials and Methods

Tetraethoxysilane (TEOS, Sigma Aldrich 99.5%), abs. ethanol (Fisher, 99.6%), hydrochloric acid (VWR, 37%), hexamethyldisilazane (HMDS, TCI Chemicals, >96.0%), cetyltrimethylammonium bromide (CTAB, Sigma Aldrich, 99%), sodium thiocyanate (Fluka, p.a.), benzonitrile (Sigma Aldrich, 99 %), and valeronitrile (Sigma Aldrich, 99%) were used as received. Abs. acetone (Sigma Aldrich, 99 %) was dried over molar sieves. Nitrile rubber gloves were obtained from VWR. Aqueous nitrile and NaSCN solutions were prepared by weight.

Synthesis of Mesoporous Surface-Modified Silica

The synthesis of mesoporous surface-modified silica was adapted from the literature.[31–33] The sol was prepared by the addition of 0.9 mL water (pH = 1.25 adjusted with HCl) to 2.08 g TEOS diluted in 2.2 mL ethanol. The mixture was stirred at 40 °C for 3 h. For 3D hexagonal structures and for cubic structures, 0.12 eq and 0.16 eq CTAB (0.041 g or 0.054 g), respectively, were dissolved in 0.5 mL ethanol, followed by addition of 0.5 mL, leading to a final molar ratio of 1:13:5:5 × 10^{-3}:0.12–0.16 for TEOS:EtOH:H_2O:HCl:CTAB. The mixture was stirred for 5 min and spin coated onto the Si ATR crystals with a spinner velocity of 2000 rpm. The RH of the spinner chamber was controlled and adjusted to 50% for the 3D hexagonal structures and to 65% for the cubic structures. Prior to deposition, the ATR crystals were ultrasonically cleaned with ethanol and dried in a nitrogen flow. After deposition, the samples were pretreated at 110 °C overnight, followed by further drying *en vacuu* at 150 °C for 2 h. For simultaneous surfactant removal and surface modification, 20 mL abs. acetone and 0.5 mL HMDS were added to the ATR crystals under inert atmosphere and the mixture was heated to reflux temperature for 4 h. The modified films were thoroughly washed with acetone and dried at 110 °C overnight.

Characterization of Mesoporous Surface-Modified Silica

Low Angle X-ray diffraction data was collected with an Empyrean PANanalytical multipurpose diffractometer in Bragg-Brentano geometry operating with a Cu anode at 45 Kv and 40 mA; a GalliPix detector was used. Samples were placed on the silicon single crystal sample holder. The diffraction patterns were recorded at room temperature between 1° and 6° (2θ) at a rate of 100 s/step and a step size of 0.01°. The sample holder was rotated during measurements at a rate of 4 s/turn. Transmission spectra were recorded on a Bruker Tensor 27 FTIR spectrometer. Experiments were performed with a custom-made liquid cell comprising two 2 mm-thick CaF_2 windows separated by an 11.4 µm-thick PTFE spacer. Contact angles were measured on a Krüss DSA 30 contact angle goniometer equipped with a video camera. Static contact angles were obtained with the tangent method of the instrument software from 10 µL water droplets that were placed onto the sample's surface. Transmission electron microscopy (TEM) of cross-section specimens was performed on a FAI TECNAI G20 operating at 200 keV. Film thickness was determined via a Bruker Dektak XTL Stylus profilometer by measuring five scratches distributed over the entire film for several coatings.

The variation of the thickness within a single film as well as the film-to-film variation was ±10 nm (e.g., for different 3D hexagonal films: 425, 441, 425, 426, and 424 nm) except for the 1 mm rims, which based on the flow cell design are not in contact with the sample.

Optical Setup

Adapted from Karabudak et al.,[37] 10 mm × 20 mm silicon ATR crystals were cut with a dicing machine from standard low resistivity ~525 µm thick, double-side polished CZ Si wafers. The narrow facets were polished to a defined angle of 55°. This angle of incidence allowed for 14 active internal reflections within the ATR crystal.[20] The ATR crystals were inserted into a home-built 20 µL aluminum flow cell. A FKM O-ring formed a watertight seal around the edges of the ATR crystals. The flow cell setup was placed in the sample compartment of a Bruker Vertex 80v spectrometer equipped with a liquid nitrogen cooled mercury–cadmium–telluride (MCT) detector (InfraRed Associates, $D^* = 4 \times 10^{10}$ cm $Hz^{0.5}$ W^{-1} at 9.2 µm). Two gold mirrors directed the IR beam onto the angled facets and detector, respectively (see Scheme 2). IR spectra were acquired with a spectral resolution of 4 cm^{-1}, and a total of 8–32 scans (1–4 s, double-sided, backward forward acquisition mode) were averaged per spectrum. The beam diameter was optimized for maximum signal at the MCT detector and minimal noise, resulting in an optimal beam aperture of 8 mm. The noise level was evaluated as the RMS of 100% lines, which were obtained by calculating the absorbance spectrum of two subsequent single-beam spectra of the same sample under identical conditions (see Supporting Information for spectra). The RMS noise between 2200 and 2000 cm^{-1} was determined to be 4×10^{-5} AU from 32 averaged scans (4 s scan time).

Spectra analysis was performed using the software package OPUS 7.5 (Bruker Corp., Ettlingen, Germany) and a Matlab script that was used for linear baseline subtraction and integration of absorption bands.

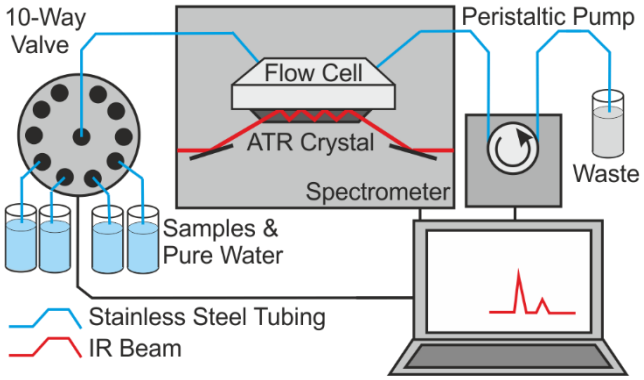

Scheme 2. Optical setup consisting of a flow cell placed on a Si ATR crystal within a commercial FTIR spectrometer. The sample is supplied by an automated flow system comprising a peristaltic pump and a selection valve.

Liquid Handling and Sampling

An automated flow system enabled reproducible sample application. The system consists of a 10-way selection valve (Valco Instruments Co. Inc., Schenkon, Switzerland), a peristaltic

pump (Ismatec), and 1/16-in. stainless steel tubing with 1 mm inner diameter. The distance between selection valve and flow cell was 30 cm. Stainless steel tubing was used instead of tubing made of plastic to avoid possible absorptions of the organic substances into polymer tubing walls. A LabView-based GUI (National Instruments) with server-client program structure controlled the system.[38] Pure water and benzonitrile solutions with different concentrations were applied at a flow rate of 2 mL min^{-1}. For equilibrium adsorption experiments, the flow cell was flushed for 2 min.

AUTHOR INFORMATION

Corresponding Author

*Email: bernhard.lendl@tuwien.ac.at

Author Contributions

All authors contributed to the writing of this manuscript, and all authors have given approval to the final version of the manuscript.

ACKNOWLEDGMENT

This work is part of the AQUARIUS project, which has received funding from the European Union's Horizon 2020 research and innovation program under grant agreement No. 731465. This project is an initiative of the Photonics Public Private Partnership. J.H. acknowledges funding from the Competence Centre ASSIC – Austrian Smart Systems Research Center – within the COMET – Competence Centers for Excellent Technologies program. X-ray diffraction was performed at the interfaculty X-Ray Center of TU Vienna. TEM measurements were performed at USTEM. B.B. acknowledges the group of Prof. Strasser for help with ATR crystal preparation.

REFERENCES

1. Kresge, C.; Leonowicz, M.; Roth, W.; Vartuli, J. Ordered Mesoporous Molecular Sieves Synthesized by a Liquid-Crystal Template Mechanism. *Nature* **1992,** *359,* 710–712.

2. Hoffmann, F.; Cornelius, M.; Morell, J.; Fröba, M. Silica-Based Mesoporous Organic-Inorganic Hybrid Materials. *Angew. Chem., Int. Ed.* **2006,** *45*, 3216–3251.

3. Wan, Y.; Zhao, D. On the Controllable Soft-Templating Approach to Mesoporous Silicates. *Chem. Rev.* **2007,** *107*, 2821–2860.

4. Nicole, L.; Boissière, C.; Grosso, D.; Quach, A.; Sanchez, C. Mesostructured Hybrid Organic–Inorganic Thin Films. *J. Mater. Chem.* **2005,** *15*, 3598–3627.

5. Rouquerol, J. *et al.* Recommendations for the Characterization of Porous Solids. *Pure Appl. Chem.* **66,** 1739–1758 (1994).

6. Brunel, D.; Blanc, A. C.; Galarneau, A.; Fajula, F. New Trends in the Design of

Supported Catalysts on Mesoporous Silicas and Their Applications in Fine Chemicals. *Catal. Today* **2002,** *73*, 139–152.

7. Clark, J. H.; Macquarrie, D. J.; Tavener, S. J. The Application of Modified Mesoporous Silicas in Liquid Phase Catalysis. *Dalt. Trans.* **2006,** *0*, 4297.

8. Macquarrie, D. J. Organically Modified Micelle Templated Silicas in Green Chemistry. *Top. Catal.* **2009,** *52*, 1640–1650.

9. Walcarius, A.; Collinson, M. M. Analytical Chemistry with Silica Sol-Gels: Traditional Routes to New Materials for Chemical Analysis. *Annu. Rev. Anal. Chem.* **2009,** *2*, 121–143.

10. Walcarius, A.; Mandler, D.; Cox, J. A.; Collinson, M.; Lev, O. Exciting New Directions in the Intersection of Functionalized Sol–Gel Materials with Electrochemistry. *J. Mater. Chem.* **2005,** *15*, 3663–3689.

11. Melde, B. J.; Johnson, B. J.; Charles, P. T. Mesoporous Silicate Materials in Sensing. *Sensors* **2008,** *8*, 5202–5228.

12. Scott, B. J.; Wirnsberger, G.; Stucky, G. D. Mesoporous and Mesostructured Materials for Optical Applications. *Chem. Mater.* **2001,** *13*, 3140–3150.

13. Clark, J. H.; Macquarrie, D. J.; Wilson, K. Functionalised Mesoporous Materials for Green Chemistry. *Stud. Surf. Sci. Catal.* **2000,** *129*, 251–264.

14. Walcarius, A.; Mercier, L. Mesoporous Organosilica Adsorbents: Nanoengineered Materials for Removal of Organic and Inorganic Pollutants. *J. Mater. Chem.* **2010,** *20*, 4478–4511.

15. Zhu, D.; Zhang, H.; Tao, Q.; Xu, Z.; Zheng, S. Surface Functionalized Mesoporous Silicas as Adsorbents for Aromatic Contaminants in Aqueous Solution. *Environ. Toxicol. Chem.* **2009,** *28*, 1400–1408.

16. Qin, Q.; Xu, Y. Enhanced Nitrobenzene Adsorption in Aqueous Solution by Surface Silylated MCM-41. *Microporous Mesoporous Mater.* **2016,** *232*, 143–150.

17. Sepehrian, H.; Fasihi, J.; Khayatzadeh Mahani, M. Adsorption Behavior Studies of Picric Acid on Mesoporous MCM-41. *Ind. Eng. Chem. Res.* **2009,** *48*, 6772–6775.

18. Anbia, M.; Lashgari, M. Synthesis of Amino-Modified Ordered Mesoporous Silica as a New Nano Sorbent for the Removal of Chlorophenols from Aqueous Media. *Chem. Eng. J.* **2009,** *150*, 555–560.

19. Gowen, A. A.; Tsenkova, R.; Bruen, M.; Odonnell, C. Vibrational Spectroscopy for Analysis of Water for Human Use and in Aquatic Ecosystems. *Crit. Rev. Environ. Sci. Technol.* **2012,** *42*, 2546–2573.

20. Ramer, G.; Lendl, B. In *Encyclopedia of Analytical Chemistry*; John Wiley & Sons, 2013.

21. Yang, J.; Cheng, M. L. Development of an SPME/ATR-IR Chemical Sensor for Detection of Phenol Type Compounds in Aqueous Solutions. *Analyst* **2001,** *126*, 881–886.

22. Göbel, R.; Krska, R.; Kellner, R.; Seitz, R. W.; Tomellini, S. A. Investigation of Different Polymers as Coating Materials for IR/ATR Spectroscopic Trace Analysis of Chlorinated Hydrocarbons in Water. *Appl. Spectrosc.* **1994,** *48*, 678–683.

23. Dobbs, G. T.; *et al.* Mid-Infrared Chemical Sensors Utilizing Plasma-Deposited Fluorocarbon Membranes. *Anal. Chem.* **2007,** *79*, 9566–9571.

24. Schädle, T.; Pejcic, B.; Myers, M.; Mizaikoff, B. Fingerprinting Oils in Water via Their Dissolved VOC Pattern using Mid-Infrared Sensors. *Anal. Chem.* **2014,** *86*, 9512–9517.

25. Lu, R.; *et al.* Determination of Chlorinated Hydrocarbons in Water Using Highly Sensitive Mid-Infrared Sensor Technology. *Sci. Rep.* **2013,** *3*, 1–6.

26. Lu, Y.; Han, L.; Brinker, C. J.; Niemczyk, T. M.; Lopez, G. P. Chemical Sensors Based on hHydrophobic Porous Sol-Gel Films and ATR-FTIR Spectroscopy. *Sens. Actuators, B* **1996,** *36*, 517–521.

27. Janotta, M.; Karlowatz, M.; Vogt, F.; Mizaikoff, B. Sol-Gel Based Mid-Infrared Evanescent Wave Sensors for Detection of Organophosphate Pesticides in Aqueous Solution. *Anal. Chim. Acta* **2003,** *496*, 339–348.

28. Ciriminna, R.; *et al.* The Sol-Gel Route to Advanced Silica-Based Materials and Recent Applications. *Chem. Rev.* **2013,** *113*, 6592–6620.

29. Lovecka, P.; *et al.* Study of Cytotoxic Effects of Benzonitrile Pesticides. *Biomed Res. Int.* **2015,** *2015*, 1–9.

30. Brinker, J. C.; Lu, Y.; Sellinger, A.; Fan, H. Evaporation-Induced Self-Assembly: Nanostructures Made Easy. *Adv. Mater.* **1999,** *11*, 579–585.

31. Besson, S.; Gacoin, T.; Ricolleau, C.; Jacquiod, C.; Boilot, J.-P. Phase Diagram for Mesoporous CTAB–Silica Films Prepared Under Dynamic Conditions. *J. Mater. Chem.* **2002,** *13*, 404–409.

32. Matheron, M.; *et al.* Highly Ordered CTAB-Templated Organosilicate Films. *J. Mater. Chem.* **2005,** *15*, 4741–4745.

33. Matheron, M.; Gacoin, T.; Boilot, J.-P. Stabilization of Well-Organized Transient Micellar Phases in CTAB-Templated Silica and Organosilica Thin Films. *Soft Matter*

2007, *3*, 223–229.

34. Ho, Y. S. Selection of Optimum Sorption Isotherm. *Carbon N. Y.* **2004,** *42*, 2115–2116.

35. Mirabella, F. M. *Internal Reflection Spectroscopy: Theory and Applications*; Marcel Dekker, 1993.

36. Kischkat, J.; *et al.* Mid-Infrared Optical Properties of Thin Films of Aluminum Oxide, Titanium Dioxide, Silicon Dioxide, Aluminum Nitride, and Silicon Nitride. *Appl. Opt.* **2012,** *51*, 6789–6798.

37. Karabudak, E.; *et al.* Disposable Attenuated Total Reflection-Infrared Crystals from Silicon Wafer: A Versatile Approach to Surface Infrared Spectroscopy. *Anal. Chem.* **2013,** *85*, 33–38.

38. Wagner, C.; Genner, A.; Ramer, G.; Lendl, B. Advanced Total Lab Automation System (ATLAS). In *Modeling, Programming and Simulations Using LabVIEW Software*; InTech Open, 2011.

TOC